Modeling single arm electron scattering and nucleon production from nuclei by GeV electrons

J. W. Lightbody, Jr.[a)]
National Science Foundation, Washington, DC 20006

J. S. O'Connell
National Bureau of Standards, Gaithersburg, Maryland 20899

(Received 7 December 1987; accepted 25 January 1988)

Nuclear reaction data for the doubly differential cross sections of inelastic electron scattering and of electronucleon and electropion production are parametrized by analytic models of the major reaction mechanisms. Predictive FORTRAN codes for the yields of reaction products have been developed for all nuclei interacting with electrons and bremsstrahlung beams in the energy range 0.5–5 GeV. Comparison with a variety of electromagnetic reaction data is shown.

INTRODUCTION

Parametrization of inelastic electron scattering (e,e') and electronucleon production (e,N) cross sections for nuclei is a convenient tool for the design of nuclear physics experiments and in the analysis of the resulting data. For example, to make radiative corrections to electron scattering data at one value of momentum and energy transfer one needs the value of the scattering cross section at lower energy transfers for a variety of momentum transfers. A parametrization of the (e,e') cross section provides this.

A second example is the use of the (e,e') and (e,N) single arm cross sections in assessing the feasibility of a $(e,e'N)$ coincidence measurement. The singles rates in both arms and the accidental coincidences between arms rates are important practical considerations. Parametrized cross sections are also useful in calculating other types of experimental backgrounds (from target walls, target backings, etc.). In this article we develop a computer program (written in FORTRAN 77) to predict doubly differential cross sections for (e,e'), (e,N), and (e,π) in different nuclei.

Our aim is to be able to predict (e,e') cross sections to within 20% for an incident electron in the energy range 0.5–5 GeV and for energy losses greater than 50 MeV and to be able to predict (e,N) cross sections in the same electron energy range to within a factor of 2 for nucleon kinetic energies greater than 50 MeV.

In Sec. I a model (code QFS) for the (e,e') cross section based on five reaction mechanisms in the continuum is developed and compared to radiatively corrected data. An option of the code is to predict the data before radiative corrections have been applied, i.e., the (e,e') cross section as measured. In Sec. II electronucleon production is modeled (code EPC) using three reaction mechanisms. An argument is made that for our purposes final state interactions of nucleons emerging from the nucleus will not make large corrections to our predictions. Other codes that handle this correction are cited. In Sec. III the yields of nucleons from bremsstrahlung beams is modeled (code GPC) using two of the mechanisms discussed in Sec. II. Pion production by electron and bremsstrahlung beams is discussed in Sec. IV. Finally, in Sec. V we discuss the availability of our codes.

The kinematic notation to be followed is illustrated in Fig. 1. An incident electron of momentum $\mathbf{k}$ and energy E scatters from a nucleus of atomic weight A with Z protons and N neutrons $(A = Z + N)$. If the scattered electron $(\mathbf{k}',E')$ is detected in an (e,e') measurement at an angle θ with respect to the incident electron direction, then the three-momentum and energy transfer to the nucleus are

$$\mathbf{q} = \mathbf{k} - \mathbf{k}',$$
$$\omega = E - E'. \tag{1}$$

The square of the four-momentum transfer is

$$Q^2 = q^2 - \omega^2. \tag{2}$$

For real photons $q^2 = \omega^2$ so $Q^2 = 0$.

If a nuclear reaction product x is detected in an (e,x) measurement (x = proton, neutron, pion) its momentum $\mathbf{p}_x$, kinetic energy T_x, and total energy are related relativistically by

$$E_x = (p_x^2 + m_x)^{1/2} = T_x + m_x, \tag{3}$$

where m_x is either the nucleon mass M or pion mass m_π. The invariant mass of a particle or group of particles is defined as

$$W_x = (E_x^2 - p_x^2)^{1/2}. \tag{4}$$

Variables in the center-of-momentum system of a virtual or real photon and a nucleon are labeled with a superscript cm, otherwise the lab system is assumed. A Lorentz transformation relates the two systems. Atomic units are used: $\hbar = c = 1$.

I. INCLUSIVE ELECTRON SCATTERING CROSS SECTIONS

We have developed a phenomenological model to approximate the inclusive (e,e') cross section. The model assumes largely incoherent electron–nucleon scattering. We retain the essential physical processes known to contrib-

[a)] Permanent address: National Bureau of Standards.

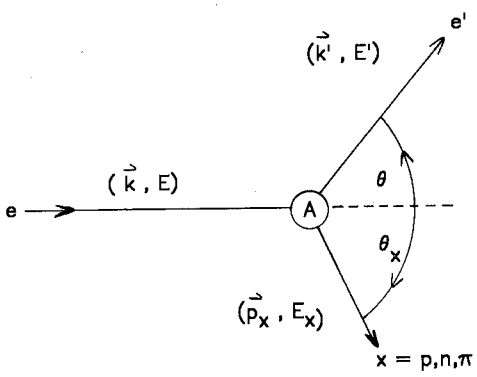

FIG. 1. Kinematic variables used for inelastic electron scattering (e,e') and for electroproduction (e,x).

ute to the inclusive cross section, including the following: (1) quasielastic (e,e') scattering on a bound nucleon, (2) scattering on two interacting nucleons, (3) Δ electroproduction, (4) higher nucleon resonance electroproduction (two resonances, one centered at an invariant mass of $W = 1500$ MeV, and another centered at $W = 1700$ MeV), and (5) deep inelastic (e,e') in the X-scaling regime. As a constraint, we require that this model approximately reproduce the real photon total absorption cross section. The model does not apply to low-energy electron scattering, i.e., momentum transfers below the Fermi momentum, or energy losses in the domain of coherent nuclear excitations.

The quasielastic region is described as a Gaussian in electron energy loss (ω), centered at $Q^2/(2M) + \epsilon_s$, where ϵ_s is the mean separation energy, and with a width proportional to qk_F/M. The low- and high-energy loss tails of this distribution better describe the experimental data than the zero temperature Fermi gas model. The integrated cross section is constrained to yield the sum of incoherent eN cross sections $(Z\sigma_{ep} + N\sigma_{en})$. A dipole form factor is used to describe the momentum transfer dependence of the eN cross sections. We assume that the proton (p) and neutron (n), charge (E), and magnetic (M) form factors have the following forms:

$$G_{Ep}(Q^2) = (1 + Q^2/a_p^2)^{-2} [\equiv f_d(Q^2,a), \text{ the dipole form}],$$
$$G_{En}(Q^2) = \frac{-\mu_n Q^2/(4M^2) G_{Ep}(Q^2)}{[1 + 5.6Q^2/(4M^2)]}, \tag{5}$$
$$G_{Mp,n}(Q^2) = \mu_{p,n} G_{Ep}(Q^2).$$

The eN cross sections are written in the Rosenbluth form,

$$\sigma(\theta) = \sigma_{\text{Mott}}(\theta) \left[\frac{G_E^2 + (Q^2/4M^2)G_M^2}{1 + (Q^2/4M^2)} + \frac{Q^2}{2M^2} G_M^2 \tan^2\left(\frac{\theta}{2}\right) \right], \tag{6}$$

where the Mott cross section is

$$\sigma_{\text{Mott}}(\theta) = \left(\frac{\alpha}{2E}\right)^2 \frac{\cos^2(\theta/2)}{\sin^4(\theta/2)} \frac{1}{1 + 2(E/M)\sin^2(\theta/2)}, \tag{7}$$

with $\alpha = 1/137$.

The dipole parameter (a_p) was chosen to achieve a best fit to all available data. In doing this, it was necessary to introduce an A dependence; $a_p = 840$ MeV/c for the free nucleon and decreases linearly to 750 MeV/c for $A = 4$. Beyond $A = 4$, a_p is not changed. We make no interpretation of this observation, although it is clearly suggestive of modifications to nucleon properties inside nuclei.

The two-nucleon emission process is expected to play a role in the so-called "dip" region between the quasifree scattering peak and the Δ-electroproduction peak. We assume that, as suggested by theory, this process is dominated by isovector meson exchange currents and is transverse in nature. The form of the two-nucleon knockout component of the inclusive (e,e') cross section is as follows:

$$\sigma(Q^2,\omega,\theta) = \sigma_{\text{Mott}}(\theta) \left[\frac{Q^2}{2q^2} + \tan^2\left(\frac{\theta}{2}\right) \right] R_{2N}(Q^2,\omega). \tag{8}$$

The response function R_{2N} has the following features. The total strength in this channel is assumed to scale as NZ/A, the same as for the quasideuteron model of total photoabsorption. We introduce a Lorentzian-shaped peak, centered at an energy loss approximately halfway between the quasifree single nucleon knockout and Δ-electroproduction peaks. Threshold for this process is at $\omega_{\text{thr}} = Q^2/4M$ and corresponds to elastic scattering from the deuteron. A cutoff factor is introduced to provide a reasonable near-threshold ω dependence and to respect the threshold itself. The functional Q^2 dependence of the response function is the same as we used for Δ electroproduction. The explicit form of the response function is as follows:

$$R_{2N}(Q^2,\omega) = K_{2N}(NZ/A) q^2 f_d^2(Q^2,a_{2N}) \times \left(\frac{\Gamma_{2N}^2 W^2}{(W^2 - W_{\text{cm}}^2)^2 + \Gamma_{2N}^2 W^2} \right) \times \left[1 - \exp\left(-\frac{(\omega - \omega_{\text{thr}})}{\Gamma_{\text{thr}}} \right) \right], \quad \text{for } \omega > \omega_{\text{thr}}$$

or

$$= 0, \quad \text{for } \omega < \omega_{\text{thr}}, \tag{9}$$

where the invariant mass W, written in terms of electron energy loss, is

$$W^2 = M^2 + 2M(\omega - Q^2/2M). \tag{10}$$

The Lorentzian is centered at a single nucleon invariant mass of $W_{\text{cm}} = (M + M_\Delta)/2$. The width (Γ_{2N}) of the Lorentzian was determined in a very crude fashion from the available data and is given by a constant value of 300 MeV. We obtain a dipole scale parameter (a_{2N}) of 550 MeV/c, substantially below the free nucleon value of 840 MeV/c, yet qualitatively consistent with the larger size of quasideuteron constituents. The threshold scale factor $\Gamma_{\text{thr}} = 20$ MeV. The overall cross-section scale factor K_{2N} was determined by fitting deuteron "dip-region" data.

Turning next to the nucleon resonance region, we begin with the $\Delta(1232$ MeV) state. We again use a Lorentzian to describe this feature. The threshold region behavior is assumed to be the same as described in the previous section. The threshold is taken to be the free nucleon electropion production threshold. For complex nuclei, the threshold can be below this value because of coherence effects. We neglect this latter effect in our model. The width of the Δ resonance (Γ_Δ) has three components that are combined in quadrature:

(1) The nautral width is 110 MeV.

(2) The second component results from Fermi motion. For the Fermi gas model of quasielastic electron scat-

tering, this width is proportional to qk_F/M. The constant of proportionality for our model was determined to be approximately 1.1 by fit to $^{16}O(e,e')$ quasielastic scattering data taken at 730 MeV and $\theta = 37.1°$.

(3) The third component reflects a dependence on the nuclear medium. This component increases linearly from zero at $A = 1$, to a maximum of 140 MeV at $A = 4$.

The general functional form of the cross section is precisely as given in the previous section on two-nucleon knockout. The cross section is assumed to be totally transverse in nature. However, the dipole parameter (a_Δ) in the form factor is now different. As in the case of the width, there is now an A dependence to a_Δ required by a global fit to all available data. The value of a_Δ for the free nucleon is 774 MeV. This drops linearly to a value of 700 MeV for $A = 4$ and is assumed to remain constant thereafter. This departure from free nucleon values is consistent with the above results in the quasielastic region. An overall $A(e,e')A_\Delta$ cross-section normalization factor was derived from known proton cross sections by scaling the proton peak cross section with the ratio $\Gamma_\Delta(A=1)/\Gamma_\Delta(A)$. The peak position was fixed by kinematics to agree with the peak seen in photon absorption. An offset ϵ_Δ takes binding effects into account. Typical values found for ϵ_Δ in complex nuclei were near -15 MeV, corresponding to a shift from the free nucleon Δ-peak location to lower energy losses. This is in contrast to the observed shifts in quasielastic peak locations to energy losses greater than observed for the free nucleon, by typical values of 25 MeV. Finally, in connection with the Δ and higher energy resonances, a common value of 5 MeV was taken for the threshold region cutoff widths $\Gamma_{\rm thr}$.

From early Stanford Linear Accelerator Center (SLAC) $N(e,e')N^*$ data, we observe that the dominant higher resonances occur at invariant masses of 1500 and 1700 MeV. We include only these two states (actually, groups of states) in our model. The higher energy nucleon resonances are assumed to have functional forms identical to the Δ and two-nucleon knockout peaks. We are, therefore, assuming that the $W = 1500$ and 1700 MeV features are predominantly transverse in nature. The widths (all components) used in our model for these states are identical to those used for the Δ. The only differences occur in the dipole form factor scale parameters (a_{R1} and a_{R2} for the $W = 1500$ and 1700 MeV structures, respectively). The higher resonances fall off more slowly with Q^2 than the Δ. Also, there is no obvious A dependence to these scale parameters. We found best values of $a_{R1} = 1000$ MeV/c and $a_{R2} = 1200$ MeV/c. Using the same prescription as the Δ, the $W = 1500$ MeV and 1700 MeV cross-section normalizations were established by comparison to proton (e,e') data from SLAC.

Deep inelastic electron scattering at SLAC gave early indications of quark substructure within the nucleon. A broad structure begins at an invariant mass roughly underlying the nucleon resonances. The structure functions associated with this region reveal a correlated (Q,ω) dependence, namely, a functional dependence on a single variable, $X = Q^2/2M\omega$. This is the form that suggests scattering from pointlike constituents.

We attempted to synthesize both the (e,e') and photoabsorption data in this region. The real photon data is characterized by the broad nucleon resonances, described above, and by what appears to be a slowly rising, nonresonant "background" that underlies the resonances and that reaches a roughly constant value near 2–3 GeV. In this region the Q^2 dependence is such that the nonresonant component begins to dominate the resonances above Q^2 of roughly 1 (GeV/c)^2, until at Q^2 of 3–4 (GeV/c)^2 the resonances are barely discernable features. Besides the stronger Q^2 dependence of the resonances compared to the background, the resonances have broadened out due to Fermi motion and, for the heavier nuclei, additional damping width due to medium effects.

We chose to describe the various data in terms of a virtual photon flux factor, a virtual photon cross section (depending on ω), and a form factor (depending on Q^2). The nuclear scaling region cross section is taken to be A times the free nucleon scattering cross section. The resultant expression for the nuclear electron scattering cross section is as follows:

$$\sigma = \Gamma_v \sigma_\gamma(\omega)(1 + \epsilon R_x)F_x^2(Q^2), \tag{11}$$

where Γ_v is the virtual photon flux,

$$\Gamma_v = \frac{\alpha}{2\pi^2}\frac{E'\kappa}{EQ^2}\frac{1}{1-\epsilon}, \quad \kappa = \omega - \frac{Q^2}{2M}, \tag{12}$$

$F_x(Q^2)$ is a form factor; ϵ is the virtual photon polarization, given by

$$\epsilon = [1 + (2q^2/Q^2)\tan^2(\theta/2)]^{-1}. \tag{13}$$

Functionally, the photon polarization vanishes as the real photon point ($Q^2 = 0$) is approached; ϵ is a measure of the ratio of longitudinal to transverse photon flux in the effective photon beam. Here R_x is the ratio of longitudinal to transverse cross sections. Recent SLAC measurements of R_x show a substantial Q^2 dependence and support the following parametrization:

$$R_x = 0.56 \times 10^6 \ (\text{MeV}/c)^2/(Q^2 + M_N^2). \tag{14}$$

The real photon cross section is parametrized using the following form:

$$\sigma_\gamma(\omega) = \left(\sigma_0 + \frac{\sigma_1}{(\omega - \omega_\pi)}\right)\left[1 - \exp\left(-\frac{(\omega-\omega_\pi)^2}{(2\Gamma_x^2)}\right)\right], \tag{15}$$

where $\sigma_0 = 100$ μb and $\sigma_1 = 54 \times 10^3$ μb MeV. Threshold for the photon cross section ω_π is taken to be at the free nucleon pion electroproduction threshold,

$$\omega_\pi = Q^2/(2M) + m_\pi + m_\pi^2/(2M). \tag{16}$$

The width parameter $\Gamma_x = 650$ MeV was determined by a rough fit to the free nucleon photodata. The constancy of the large-energy-transfer, real photon cross section is not fully reconciled with the observed scaling behavior of the electron scattering data.

To what extent this overall functional form can describe the available electron data (the real photon data are obviously given correctly, since they are used as input) is best answered by examining the resultant phenomenological form factor (F_x) one obtains for $^1H(e,e')$ at different invariant masses. In the kinematic region of interest to us, below 5–10 GeV electrons, we chose to use the following sum-of-exponentials fit to this form factor,

$$F_x^2(Q^2) = a_1 \exp(-a_2Q^2) + a_3 \exp(-a_4Q^2) + a_5 \exp[-a_6(Q^2 - a_7)^2], \tag{17}$$

where the constants were determined to be $a_1 = 0.55$, $a_2 = 20$ (GeV/c)$^{-2}$, $a_3 = 0.45$, $a_4 = 0.45$ (GeV/c)$^{-2}$, $a_5 = 0.03$, $a_6 = 0.2$ (GeV/c)$^{-4}$, and $a_7 = 4.5$ (GeV/c)^2. At the level of 20% this fit provides a reasonable description of the available data. We find this parametrization does a better job at low Q^2 than one based solely on X scaling.

A. Radiative effects

Since the idea of this modeling of cross sections is to provide a convenient and general means to estimate counting rates for inclusive electron scattering, it is important to include radiative effects as well as nuclear processes. When electrons scatter they radiate, and thus provide a purely electromagnetic mechanism for electron energy loss. We include here a description of the continuum radiation processes. These processes distort the purely nuclear processes. We do not treat the coherent radiation effects from the elastic scattering process, nor do we treat any two-step effects, which depend on the square of the target thickness. In effect we do the inverse of so-called radiative corrections and radiation tail subtractions. Our treatment of the radiation tail is within the framework of the "peaking" approximation, in which photon emission is confined to the direction of the initial or scattered electron.

The expression for the peaking approximation radiation tail is as follows:

$$d\sigma = \left[\sigma(E,\theta,\omega')\frac{\alpha}{\pi}\frac{d\omega'}{\omega-\omega'} \times\left(\log\frac{Q_1^2}{m_e^2}-1\right)\left(\frac{(E-\omega')^2+(E-\omega)^2}{2(E-\omega')^2}\right) + \sigma(E-\omega+\omega',\theta,\omega')\frac{\alpha}{\pi}\frac{d\omega'}{\omega-\omega'}\left(\log\frac{Q_2^2}{m_e^2}-1\right) \times\left(\frac{E^2+(E-\omega+\omega')^2}{2E^2}\right)\right](1+\bar{\delta}_2)\left(\frac{\omega-\omega'}{\bar{E}}\right)^{\bar{\delta}_2}, \tag{18}$$

where

$$\bar{\delta}_1 = \frac{2\alpha}{\pi}\left(\log\frac{\bar{Q}^2}{m_e^2}-1\right),$$

$$\bar{\delta}_2 = \frac{2\alpha}{\pi}\left(\frac{13}{12}\left(\log\frac{\bar{Q}^2}{m_e^2}-1\right) - \frac{17}{36} - \frac{1}{2}\left\{\frac{\pi^2}{6} - L_2\left[\cos^2\left(\frac{\theta}{2}\right)\right]\right\}\right), \tag{19}$$

$$Q_1^2 = 4E(E-\omega')\sin^2(\theta/2),$$

$$Q_2^2 = 4(E-\omega+\omega')(E-\omega)\sin^2(\theta/2),$$

$$\bar{Q}^2 = (Q_1^2 Q_2^2)^{1/2}, \quad \bar{E} = [(E-\omega)(E-\omega')]^{1/2},$$

and L_2 is Spence's integral ($n = 2$).

We integrate this expression for the radiation tail over nuclear excitations less than the energy loss of interest (ω), to begin with, from $\omega' = 0$ to $\omega' = \omega - \Delta E$. This integrated cross section describes the combination of radiation of *hard* photons and nuclear excitation by all electrons that then appear in the infinitesimal energy bin of interest. The contribution from those electrons, which suffer energy loss by a combination of *soft* photon emission and nuclear excitation in the interval $\omega' = \omega - \Delta E$ to ω, is given by the Schwinger radiative correction

$$\sigma_s = \sigma(E,\theta,\omega)(1+\delta_2)\left(\frac{\Delta E}{[E(E-\omega)]^{1/2}}\right)^{\delta_1}, \tag{20}$$

where

$$\delta_1 = \frac{2\alpha}{\pi}\left(\log\frac{Q^2}{m_e^2}-1\right), \tag{21}$$

$$\delta_2 = \frac{2\alpha}{\pi}\left(\frac{13}{12}\left(\log\frac{Q^2}{m_e^2}-1\right) - \frac{17}{36} - \frac{1}{2}\left\{\frac{\pi^2}{6} - L_2\left[\cos^2\left(\frac{\theta}{2}\right)\right]\right\}\right). \tag{22}$$

Since there are no electrons that suffer zero radiation loss, the full radiative cross section is the sum of the hard and soft photon expressions given above. For the present purposes a value of $\Delta E = 10$ MeV was chosen.

In conjunction with the subject of radiative corrections, it is worth noting that radiative effects are generally unfolded from experimental electron scattering data prior to comparison with theory. Radiatively corrected data at lower energy loss, as well as lower momentum transfer, are required to accomplish this end. The present model may prove useful in the absence of such lower (q,ω) data, or in filling in missing data by interpolation.

B. Comparisons with data

We have made comparison of the present phenomenological model with (e,e') data from the MIT/Bates linear accelerator (Linac), from SLAC, from the SLAC/nuclear physics at Stanford (NPAS) facility, and from the Deutsches elektronen-synchrotron (DESY). Comparison with real photon work was made for data from SLAC and from the Saclay Linac. Some results are shown in Figs. 2–5.[1–3] In all cases the radiation effects have been removed.

II. ELECTRONUCLEON PRODUCTION

The $d^2\sigma(e,N)$ cross sections are based on a model calculation that includes three reaction mechanisms that generate nucleons in the continuum: virtual photon absorption by bound neutron–proton pairs in the nucleus (the quasideuteron mechanism), pion production from a bound nucleon producing a free nucleon, and quasifree nucleon knockout by electron scattering. The quasideuteron and pion production processes are computed using virtual photon theory[4,5] and a parametrization of the corresponding photon differential cross sections. The knockout cross section is based on a model nucleon spectral function inserted in the quasifree impulse approximation formula. The coincidence cross section is then integrated over the angles of the unobserved scattered electron.

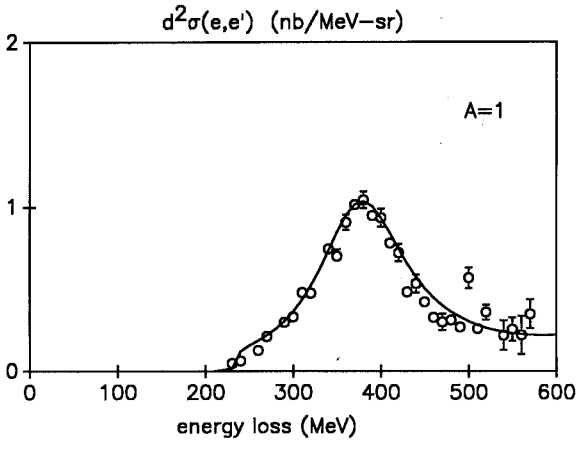

FIG. 2. Comparison of the QFS model with data[1] for 730 MeV electrons scattered at 37 deg on hydrogen in the delta region.

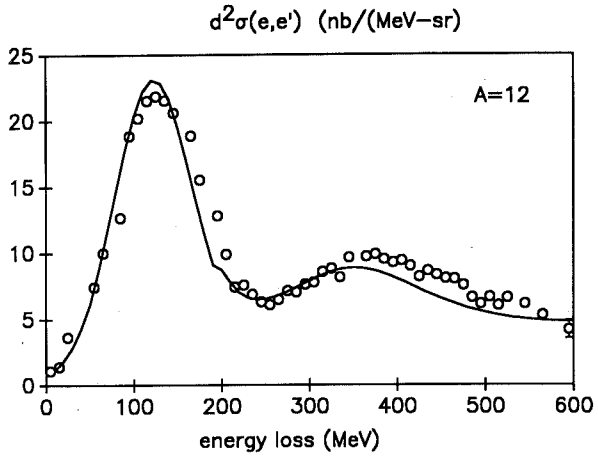

FIG. 3. Comparison of the QFS model with data[1] for 730 MeV electrons scattered at 37 deg on carbon in the quasifree, dip, and delta regions.

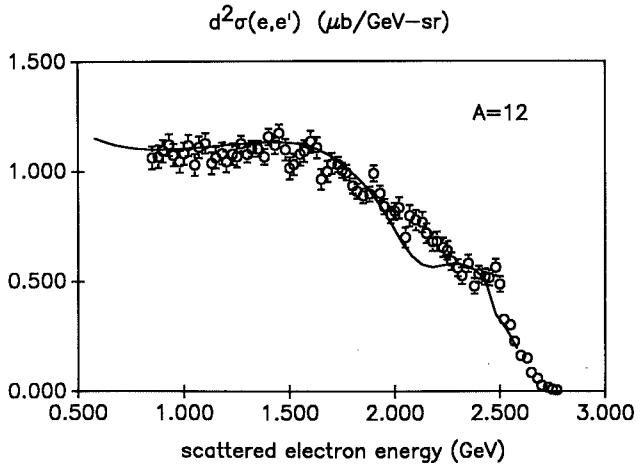

FIG. 5. Comparison of QFS model with data[3] for 3.08 GeV electrons scattered at 22 deg on carbon in the resonance and scaling regions.

A. Quasideuteron mechanism

The angular distribution of inelastically scattered electrons is usually highly peaked in the forward scattering direction. When the reaction mechanism that caused the electron to scatter also generates a corresponding real photon absorption cross section, the forward peaking approximation can be used to write the electron scattering cross section as the product of the photon cross section times the flux of virtual photons accompanying the incident electron:

$$\frac{d^2\sigma(e,N)}{d\Omega_N\, dT_N} = \frac{N_e(E,\omega)}{\omega}\frac{d\sigma(\gamma,N)}{d\Omega_N}\frac{\partial\omega}{\partial T_N}, \tag{23}$$

where ω is the laboratory photon energy required to produce the reaction product with kinetic energy T_N at the lab angle θ_N. The quantity N_e/ω is the virtual photon flux (per unit of photon energy). The partial derivative converts the final cross section to per unit particle kinetic energy. We use the virtual photon spectrum for two-body breakup given in Ref. 6.

The quasideuteron model of photon absorption assumes that the cross section is proportional to the absorption cross section of the deuteron with a constant of proportionality L (the Levinger factor) taken from experiment[7] for the particular nucleus involved:

$$\frac{d\sigma_{QD}(\gamma,N)}{d\Omega_N} = L\frac{NZ}{A}\frac{d\sigma_D(\gamma,N)}{d\Omega_N}. \tag{24}$$

The deuteron cross section itself is taken from a phenomenological fit[8] to the data for photon energies 10–625 MeV in the laboratory. Above 625 MeV we assume an isotropic angular distribution in the cm system with the cross sections given in Table I and then transformed to the laboratory system.

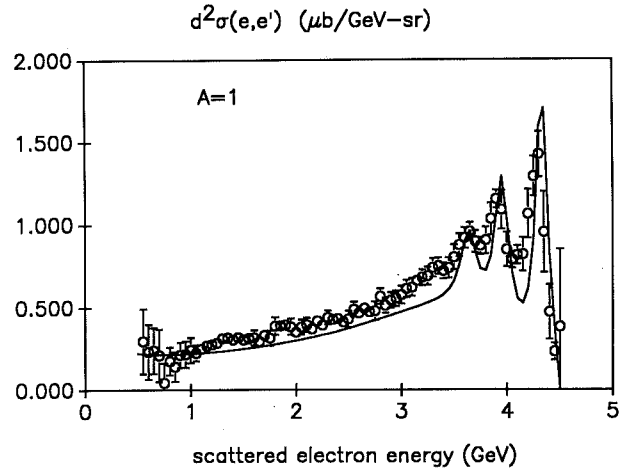

FIG. 4. Comparison of the QFS model with data[2] for 5 GeV electrons scattered at 10 deg on hydrogen in the resonance and scaling regions.

B. Recoil nucleons following pion production

Virtual photon theory is also used to predict the yield of nucleons following pion production. The virtual photon spectrum is taken from Ref. 9. The photopion cross section is based on a model in which all pions are produced through the delta resonance with an angular distribution characteristic of an angular momentum $1/2^+ \Rightarrow 3/2^+ \Rightarrow 1/2^+$ chain and appropriate isospin coupling coefficients. In the nucleon center of momentum, the photon energy dependence is parametrized by

$$\frac{d\sigma_\Delta}{d\Omega^{\rm cm}} = \frac{\sigma_1}{16\pi}\frac{(5-3\cos^2\theta^{\rm cm})}{[1+(\omega-\omega_1)^2/\Gamma^2]},$$

$$\text{if } \omega < \omega_2 \text{ or}$$

$$= \frac{(\sigma_2/4\pi)}{(1+\omega_2/\omega)},$$

$$\text{if } \omega > \omega_2, \tag{25}$$

TABLE I. Deuteron photodisintegration cross sections above 625 MeV assumed in our model.

ω (MeV)	$d\sigma/d\Omega^{\rm cm}$ (μb/sr)
$625 < \omega < 700$	0.30
$700 < \omega < 800$	0.15
$800 < \omega < 900$	0.10
$900 < \omega$	$55/(\omega - 350)$

where $\sigma_1 = 360$ μb/sr, $\omega_1 = 320$ MeV, $\sigma_2 = 90$ μb/sr, $\omega_2 = 420$ MeV, and $\Gamma = 100$ MeV; ω is the photon energy in the laboratory. The laboratory cross section is then given by

$$\frac{d\sigma_\Delta(\gamma,N)}{d\Omega_N} = N_N \frac{d\sigma_\Delta}{d\Omega^{\rm cm}} \frac{d\Omega^{\rm cm}}{d\Omega}. \tag{26}$$

The derivative that transforms the cross section to the laboratory system is evaluated numerically in the code.

For a nucleus with Z protons and N neutrons the effective number of nucleons for producing protons is

$$N_p = N/3 + 2Z/3 \tag{27}$$

and for producing neutrons is

$$N_n = Z/3 + 2N/3. \tag{28}$$

Center-of-momentum variables and laboratory variables are related by a Lorentz transformation.

C. Quasifree knockout

Virtual photon theory is not a suitable approximation to use for quasifree knockout of nucleons by scattered electrons because no real photon analog mechanism exists. However, the electron–nucleon fully differential cross section can be used in the impulse approximation. The expression[10] for nucleon plus bound residual nucleus breakup in the one-photon-exchange approximation is

$$\begin{aligned}\frac{d^3\sigma(e,e'N)}{d\Omega\, dT_N\, d\Omega_N} = {} & \frac{2\alpha^2}{Q^4}\frac{k'}{k} p_N E_N \\ & \times \left\{ \left[\left(\frac{Q^2}{q^2}\right)^2 (EE' + kk'\cos\theta + m^2) \right] W_L \right. \\ & + \left[\left(\frac{kk'\sin\theta}{q}\right)^2 + \frac{1}{2}Q^2 \right] W_T \\ & + \left[\frac{Q^2}{q^2}\left(\frac{kk'\sin\theta}{q}\right)(E+E') \right] W_{LT}\cos\phi_N \\ & \left. + \left[\left(\frac{kk'\sin\theta}{q}\right)^2 \right] W_{TT}\cos 2\phi_N \right\}, \end{aligned} \tag{29}$$

where the W response functions depend on Q^2, ω, p_N, θ_N, but not on ϕ_N, the dihedral angle between the electron scattering plane and the nuclear reaction plane. If we make the approximation that outgoing nucleons have no final state interactions, the W's can be expressed in terms of the bound nucleon spectral function $S(p,B)$, the probability that an initial nucleon (charge e, magnetic moment μ, and mass M) has momentum $p = |\mathbf{p}_N - \mathbf{q}|$ and removal energy B, then

$$\begin{aligned} W_L &= e^2 f_N^2 S(p,B), \\ W_T &= \left[e^2 \left(\frac{p_N}{M}\sin\theta_N\right)^2 + \frac{\mu^2 q^2}{2M^2} \right] f_N^2 S(p,B), \\ W_{LT} &= -2e^2 \left(\frac{p_N}{M}\sin\theta_N\right) f_N^2 S(p,B), \\ W_{TT} &= e^2 \left(\frac{p_N}{M}\sin\theta_N\right)^2 f_N^2 S(p,B), \end{aligned} \tag{30}$$

where $f_N(Q^2)$ is the nucleon form factor. In plane wave impulse approximation there is no contribution of the magnetic moment to the interference terms.[11]

The inclusive cross section is then given by the angular integral over the unobserved electron,

$$\frac{d^2\sigma(e,N)}{dT_N\, d\Omega_N} = \int_0^\pi \sin\theta\, d\theta \int_0^{2\pi} d\phi \frac{d^3\sigma}{d\Omega_N\, dT_N\, d\Omega}. \tag{31}$$

We assume that the nucleon kinetic energy is related to the electron energy transfer by $\omega = T_N + B$.

We chose parametrizations of the spectral function $S(p,B)$ for each nucleus at low A and for ranges of A at medium and high A. These parametrizations follow from few- or many-body calculations based on modern nucleon–nucleon potentials. See Fig. 6.

In performing the numerical integration of Eq. (31) some care must be taken in the integral over the electron polar angle θ. The cross section, differential in θ, is a rapidly varying function due to the Q^{-4} factor in the Mott cross section. We use Gaussian integration as described in Ref. 5 over three regions: 0–$2\theta_{\rm max}$, $2\theta_{\rm max}$–$100\theta_{\rm max}$, and $100\theta_{\rm max}$–π with 12 points per region. The angle $\theta_{\rm max} = m/(EE')$, where m is the mass of the electron.

We do not include final state interactions of a nucleon with spectator nucleons as the struck nucleon exits the nucleus. The reason is the following. These interactions degrade the kinetic energy and scatter the nucleon to other angles. As we shall see in the results to be presented and compared with data, the spectrum of nucleon kinetic energies (or momenta) falls exponentially. Moving nucleons from a higher energy to a lower energy via final state interactions results in a decrease (less than a factor of 2 for a mean free path of 5 fm) in the highest energy population without much of a fractional increase in the lower energy population. The angular distributions will be smeared by multiple scattering, but not by much, especially at the higher nucleon energies.

One could, in principle, add a Monte Carlo code like the internucleon cascade code[12] to account for final state interactions, or an imaginary optical model, or a QCD string code.[13] However, this would complicate the calculation tremendously without much improvement in its accuracy.

In Fig. 7 we give an example of the predictions of the EPC code broken down into the three reaction mechanisms. Note that each of the mechanisms dominates in some energy region. For the highest energy nucleons, quasifree knockout dominates. In Fig. 8[14] the prediction is compared with data. Unfortunately, few data on (e,p)

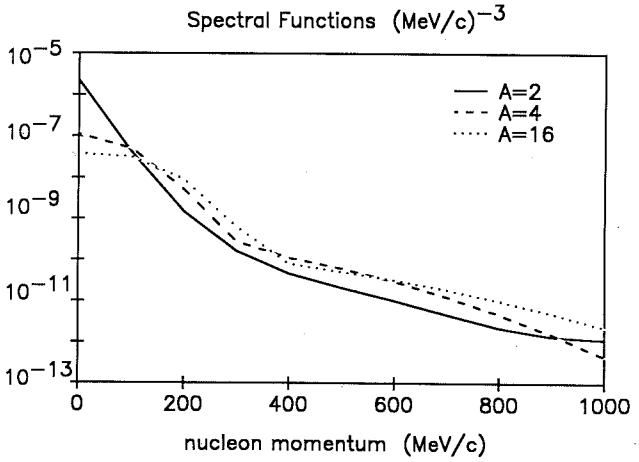

FIG. 6. Spectral functions used in the EPC model of the quasifree knockout cross sections.

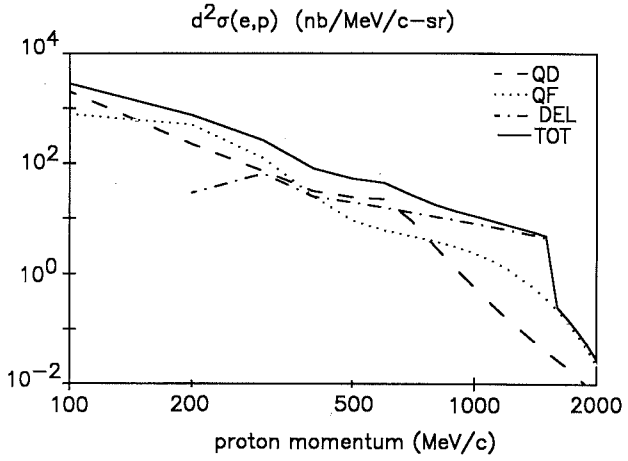

FIG. 7. Prediction of the EPC model for the proton energy spectrum produced at 45 deg by 4 GeV electrons on carbon showing the contributions of the three assumed reaction mechanisms.

cross sections are available in the literature. Charged particle yields in the forward direction (0–7°) from an 18 GeV electron beam on a variety of targets and target thicknesses are available from a series of measurements at SLAC. Although this electron energy is out of range for our models of proton production, the code EPC gives reasonable agreement with the SLAC data on thin targets. Pion yields are underestimated since only the delta region is modeled.

III. BREMSSTRAHLUNG YIELDS

Using the quasideuteron and pion production models discussed in Sec. II, we can also predict the yield of nucleons from nuclei with incident bremsstrahlung beams. The bremsstrahlung spectrum of an electron of energy E is described by

$$N_\gamma(E,\omega) = Q/\omega. \tag{32}$$

The code computes the cross section normalized to the number of bremsstrahlung equivalent quanta Q (not to be confused with four-momentum transfer, which is zero for real photons),

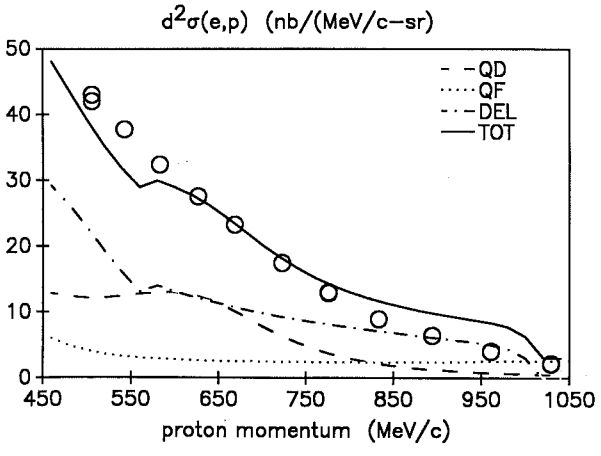

FIG. 8. Comparison of the EPC model with data[14] for a proton momentum spectrum at 17 deg for 800 MeV electrons on carbon.

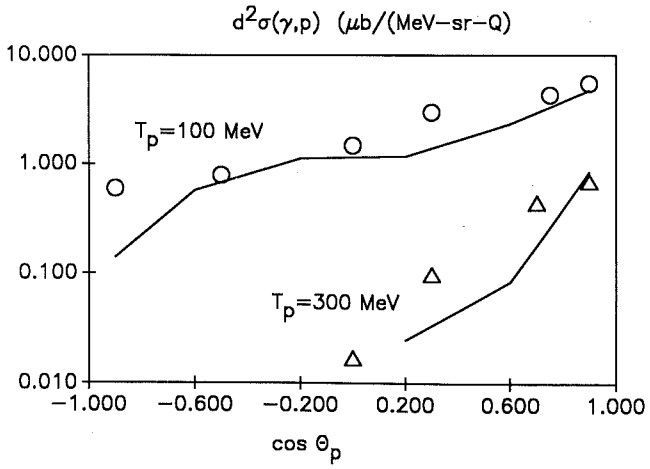

FIG. 9. Comparison of the GPC model with data[15] for proton angular distributions from 1 GeV bremsstrahlung on carbon.

$$\frac{d^2\sigma(E,T_N,\theta_N)}{Q\,d\Omega_N\,dT_N} = \frac{1}{\omega}\frac{d\sigma(\gamma,N)}{d\Omega_N}\frac{\partial\omega}{\partial T_N}. \tag{33}$$

Figures 9[15] and 10[15] show predictions of the code compared with data. We note that the accuracy of our predictions falls off at back angles and high nucleon energies where the cross sections are small. The excess yield may be due to more complicated processes as, for example, pion capture in the nucleus leading to energetic nucleons distributed isotropically. The bremsstrahlung calculations are meant as a check of the electroproduction code at lower nucleon energies where the quasideuteron and pion production process are dominant. At high nucleon energies the knockout mechanism is dominant for (e,N), thus inaccuracies in the other two minor processes are not important for the total cross section.

IV. PION YIELDS

The codes GPC and EPC also predict the cross sections for producing pions with bremsstrahlung and electrons, respectively. Both are based on single pion production from a static nucleon through the delta as discussed in Sec. II B. The effective number of nucleons for producing the three pion charges in Eq. (26) are

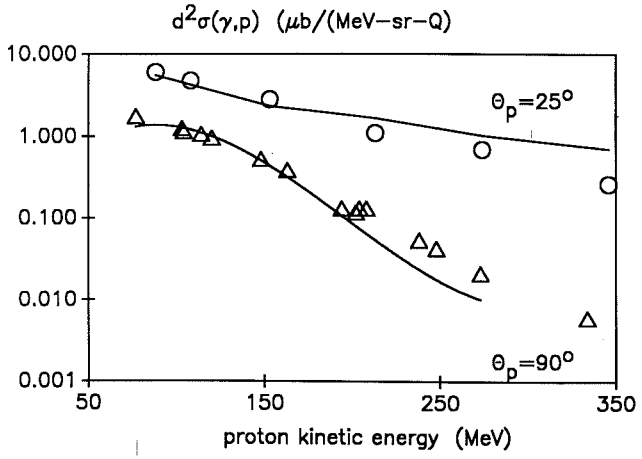

FIG. 10. Comparison of the GPC model with data[15] for proton kinetic energy distribution from 1 GeV bremsstrahlung on carbon.

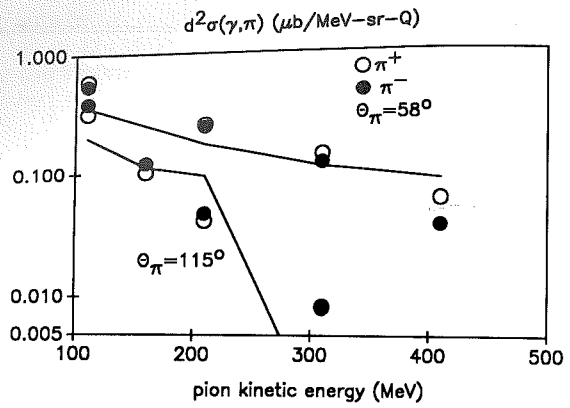

FIG. 11. Comparison of the GPC model with data[16] for charged pion kinetic energy distributions from 1 GeV bremsstrahlung on carbon.

$$N_{\pi^+} = Z/3,$$
$$N_{\pi^-} = N/3, \tag{34}$$
$$N_{\pi^0} = 2A/3.$$

The models are limited in the incident electron energy for which they are expected to be accurate since multiple pion production becomes an important mechanism above the delta resonance region. Figure 11[16] shows results for bremsstrahlung. At large angles and above an incident electron energy of 1 GeV both codes underpredict pion yields presumably because of multiple pion production.

V. DISCUSSION

The interactive codes QFS, EPC, and GPC are available from the authors. Two versions of each program exist: one suitable for running on large word length computers (e.g., CYBER with 64 bits per word), and a second suitable for running on smaller word length computers (e.g., VAX or a PC with 32 bits per word). Central processing unit (CPU) time is less than a few seconds per yield point on a PC ; however, compilation time can be several minutes. The codes are approximately 600 lines of FORTRAN for QFS and EPC, and 300 lines for GPC.

The large computer version has line numbers and operates in single precision. The second version does not have line numbers and uses double precision to achieve the same accuracy. We have tried to use portable FORTRAN statements as much as possible. All input is from the keyboard; all output is to the screen.

The codes can be obtained either by a request on BITNET to JIMOCON@NBS or by sending a formatted $5\frac{1}{4}$ in. floppy disk to the authors at RADP/B109, National Bureau of Standards, Gaithersburg, Maryland 20899.

REFERENCES

1. J. S. O'Connell, W. R. Dodge, J. W. Lightbody, Jr., X. K. Maruyama, J.-O. Adler, K. Hansen, B. Schrøder, A. M. Bernstein, K. I. Blomqvist, B. H. Cottman, J. J. Comuzzi, R. A. Miskimen, B. P. Quinn, J. H. Koch, and N. Ohtsuka, Phys. Rev. C **35**, 1063 (1987).
2. G. Mecklenbrauck, Deutsches Electronen-Synchrotron Internal Report No. F23-80/02 (unpublished).
3. U. B. Glawe, Deutsches Electronen-Synchrotron Internal Report No. F23-80/01 (unpublished).
4. R. H. Dalitz and D. R. Yennie, Phys. Rev. **105**, 1598 (1957).
5. L. Tiator and L. E. Wright, Comp. Phys. Commun. **28**, 265 (1983).
6. L. E. Wright and L. Tiator, Phys. Rev. C **26**, 2349 (1982). The expression in this article is for all partial waves. An $M1$ expression may be more appropriate for the delta.
7. J. M. Laget, *New Vistas in Electro-Nuclear Physics*, edited by E. L. Tomusiak, H. S. Caplan, and E. T. Dressler (Plenum, New York, 1986), p. 411. We use $L = 7$ for $A > 4$ and $L = A$ for $A < 4$.
8. A. E. Thorlacius and H. W. Fearing, Phys. Rev. C **33**, 1830 (1986).
9. L. Tiator and L. E. Wright, Nucl. Phys. A **379**, 407 (1982).
10. W. E. Kleppinger and J. D. Walecka, Ann. Phys. **146**, 349 (1983); **151**, 497 (1983).
11. J. S. O'Connell, Phys. Rev. C **29**, 1544 (1984).
12. T. A. Gabriel, Phys. Rev. C **13**, 240 (1976).
13. T. Sjostrand, Comp. Phys. Commun. **39**, 347 (1986).
14. R. Lourie, Massachusetts Institute of Technology Bates Laboratory (private communication).
15. D. N. Olson, Ph.D. Thesis, Cornell University, 1960 (unpublished).
16. W. M. McClelland, Phys. Rev. **123**, 1423 (1961).